

A Novel Thermal Sensor Concept for Flow Direction and Flow Velocity

Nam-Trung Nguyen, *Member, IEEE*

Abstract—This paper presents a unified theory for different measurement concepts of a thermal flow sensor. Based on this theory, a new flow sensor concept is derived. The concept allows measuring both direction and velocity of a fluid flow with a heater and an array of temperature sensors. This paper first analyzes the two-dimensional (2-D) forced convection problem with a laminar flow. The two operation modes of a constant heating power and of a constant heater temperature are considered in the analytical model. A novel estimation algorithm was derived for the flow direction. Different methods for velocity measurement were presented: the hot-wire method, the calorimetric method, and the novel average-temperature method. The only geometric parameter of the sensor, the dimensionless position of the sensor array, is optimized based on the analytical results. Furthermore, the paper presents the experimental results of the sensor prototype. In order to verify the analytical model, an array of temperature sensors was used for recording the 2-D temperature profile around the heater. Temperature values are transferred to a computer by a multiplexer. A program running on a personal computer extracts the actual flow velocity and flow direction from the measured temperature data. This paper discusses different evaluation algorithms, which can be used for this sensor. A simple Gaussian estimator was derived for the direction measurement. This estimator provides the same accuracy as the analytical estimator. Velocity results of both the calorimetric concept and the novel average-temperature concept are also presented.

Index Terms—Direction sensor, flow sensor, heat transfer, sensor array, thermal sensor.

I. INTRODUCTION

COMMERCIAL flow sensors for both direction and velocity are mainly based on a mechanical concept. The velocity and the direction are measured separately. In wind measurement, for instance, both speed sensor and direction sensor are based on the drag force. Thus, the sensor design involves moving parts, which have large sizes and require frequent maintenance. Conventional flow sensors such as Pitot probes, hot films, and hot wires are only capable of measuring point velocity [1]. Flow direction needs to be measured separately. Optical methods such as laser doppler anemometry (LDA) and particle image velocimetry (PIV) need extensive measurement setups, which are not suitable for rough, outdoor application.

The importance of thermal flow sensors for measuring the velocity and direction of a fluid flow has been recognized in experimental fluid mechanics and aerodynamics. The simplest

configuration of a thermal flow sensor is an electrically heated wire or film. This type of sensor is well established and often referred to as hot wire or hot film sensor. With the emerge of micro-machining technologies, microthermal flow sensors were recently developed [2]–[4]. The small size of these sensors makes the implementation of the highly sensitive calorimetric concept possible [5], [6]. The calorimetric concept uses the temperature difference between two positions upstream and downstream of a heater for evaluating the flow velocity. The calorimetric concept is extremely sensitive for sensors in millimeter range [7]. The major drawback of the above thermal sensors is that they can not detect flow direction. The common practice for detecting the flow direction is the use of two one-dimensional (1-D) flow sensors for measuring the two perpendicular components of the flow velocity. The inverse tangent function of the ratio between these two components is the flow direction [4], [8], [9]. The drawback of this concept is that the two 1-D flow sensors should be calibrated against each other, and very complex calibration procedures are needed.

To the best knowledge of the author, there was no unified theory for these different measurement concepts. Furthermore, no previous work identified the direct relation between the sensor sizes and the measured velocity range.

This paper first presents an unified analytical model with a laminar flow for different thermal flow sensor concepts. Based on this model, a new thermal flow sensor for both direction and velocity can be derived. This novel thermal flow sensor consists of a single heater and an array of temperature sensors. Instead of measuring a single value, the sensor collects a number of temperature values. These values are evaluated by corresponding algorithms to extract the flow direction and velocity.

Following the analytical model, this paper then presents the experimental results of a sensor prototype. The detection of the flow direction in this concept does not need any calibration. The measurement of the flow velocity can be carried out either with the calorimetric concept or with the novel average-temperature concept. The sensor presented in this paper operates in the constant heater temperature mode.

II. TWO-DIMENSIONAL SENSOR MODEL

Fig. 1 shows the model of the thermal flow sensor. The sensor consists of a circular heater. The heater can be modeled as a linear source with a heat rate of q' (W/m) [Fig. 1(a)] or with a constant temperature T_h at the heater circumference [Fig. 1(b)]. The temperature sensing array is placed on a ring with a radius R_s . For simplification, the flow direction is assumed to be $\theta_{\text{flow}} = 0$. A rotation around z axis in the Cartesian coordinate system or a translation of the direction angle θ in the cylindrical

Manuscript received November 19, 2003; revised June 30, 2004. The associate editor coordinating the review of this paper and approving it for publication was Dr. Subhas Mukhopadhyay.

The author is with the School of Mechanical and Aerospace Engineering, Nanyang Technological University, Singapore 639798 (e-mail: mntnguyen@ntu.edu.sg).

Digital Object Identifier 10.1109/JSEN.2005.858924

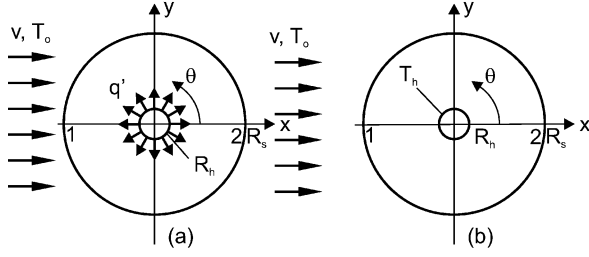


Fig. 1. Model of the thermal flow sensor for direction and velocity. (a) Constant heat rate. (b) Constant heater temperature.

coordinate system can yield the solution for the flow with a variable direction angles. The fluid flow is assumed to have a uniform velocity of v [10]. This model is similar to the Rosenthal's model of a moving heat source in a continuum [11]. This model was used for describing machining processes such as welding and laser cutting. However, the original Rosenthal's model only covers a linear point source.

The inlet temperature is the reference ambient temperature T_0 . The laminar flow with an uniform velocity can be assumed with a small Reynolds-number $Re = 2R_h v / \nu$ where ν is the kinematic viscosity of the fluid. The boundary layer effects and hydrodynamic effects behind the heater are neglected in this model.

Ignoring the source term for a homogenous form, the two-dimensional (2-D) governing equation for the temperature field of the model in Fig. 1 is

$$\frac{\partial^2 T}{\partial x^2} + \frac{\partial^2 T}{\partial y^2} = \frac{v}{\alpha} \frac{\partial T}{\partial x} \quad (1)$$

where α , defined by the thermal conductivity k , the heat capacity at constant pressure c_p , and the density ρ

$$\alpha = \frac{k}{\rho c_p} \quad (2)$$

is the thermal diffusivity of the fluid. Equation (1) can be solved using the Rosenthal's approach [10], where the temperature difference ΔT is a product of a velocity-dependent part and a symmetrical part Ψ

$$\Delta T = T - T_0 = \exp\left(\frac{vx}{2\alpha}\right) \Psi(x, y). \quad (3)$$

The substitution of

$$T = T_0 + \Delta T = T_0 + \exp\left(\frac{vx}{2\alpha}\right) \Psi(x, y) \quad (4)$$

into (1) results in

$$\frac{\partial^2 \Psi}{\partial x^2} + \frac{\partial^2 \Psi}{\partial y^2} = \left(\frac{v}{2\alpha}\right) \Psi \quad (5)$$

with the boundary conditions

$$\left. \frac{\partial \Psi}{\partial x} \right|_{x=\pm\infty} = 0, \quad \left. \frac{\partial \Psi}{\partial y} \right|_{y=\pm\infty} = 0.$$

Considering the radius $r = \sqrt{x^2 + y^2}$ around the center of the system, the boundary condition for a linear heat source is

$$\left. \frac{\partial T}{\partial r} \right|_{r=R_h} = -\frac{q'}{2\pi R_h k}.$$

In case of a constant heater temperature, the boundary condition is

$$T|_{r=R_h} = T_h.$$

Since the boundary conditions and Ψ are symmetric with respect to r ($r \geq R_h$), (5) can be formulated in the cylindrical coordinate system as

$$\frac{d^2 \Psi}{dr^2} + \frac{1}{r} \frac{d\Psi}{dr} - \left(\frac{v}{2\alpha}\right)^2 \Psi = 0. \quad (6)$$

Equation (6) is the well-know Bessel equation [12]. The solution of (6) is the modified Bessel function K_0 of the second kind and zero order [12]

$$\Psi = K_0[vr/(2\alpha)]. \quad (7)$$

In the following analysis, the results are nondimensionalised by introducing the Peclet number $Pe = 2vR_h/\alpha$ with the diameter of the heater $2R_h$ as the characteristic length. The radial variable is nondimensionalised by R_h : $r^* = r/R_h$.

A. Temperature Field With a Constant Heating Power

Considering the constant linear heat source q' (in W/m), the solution for the temperature difference is

$$\begin{aligned} \Delta T(r, \theta) &= \frac{q' \alpha}{\pi k R_h} v^{-1} \\ &\times \frac{K_0[vr/(2\alpha)]}{K_1[vR_h/(2\alpha)] - K_0[vR_h/(2\alpha)] \cos \theta} \\ &\times \frac{\exp[vr \cos \theta/(2\alpha)]}{\exp[vR_h \cos \theta/(2\alpha)]} \end{aligned} \quad (8)$$

where K_1 is the Bessel function of the second kind and first order [12]. The asymptotic case of $v = 0$ leads to the trivial case of heat conduction, where the right side of (1) becomes 0. If the dimensionless temperature difference is defined as

$$\Delta T^* = \frac{\Delta T}{2q' / (\pi k)}.$$

The dimensionless solution of the temperature field at a constant heating power is

$$\begin{aligned} \Delta T^*(r^*, \theta) &= \frac{K_0(Pe r^*/4)/Pe}{K_1(Pe/4) - K_0(Pe/4) \cos \theta} \\ &\times \{\exp[Pe(r^* - 1)/4]\}^{\cos \theta}. \end{aligned} \quad (9)$$

Fig. 2 shows this temperature field at different Peclet number.

The heater temperature is a function of θ and can be expressed in the dimensionless form as (Fig. 3)

$$\Delta T_h^*(1, \theta) = \frac{K_0(Pe/4)/Pe}{K_1(Pe/4) - K_0(Pe/4) \cos \theta}. \quad (10)$$

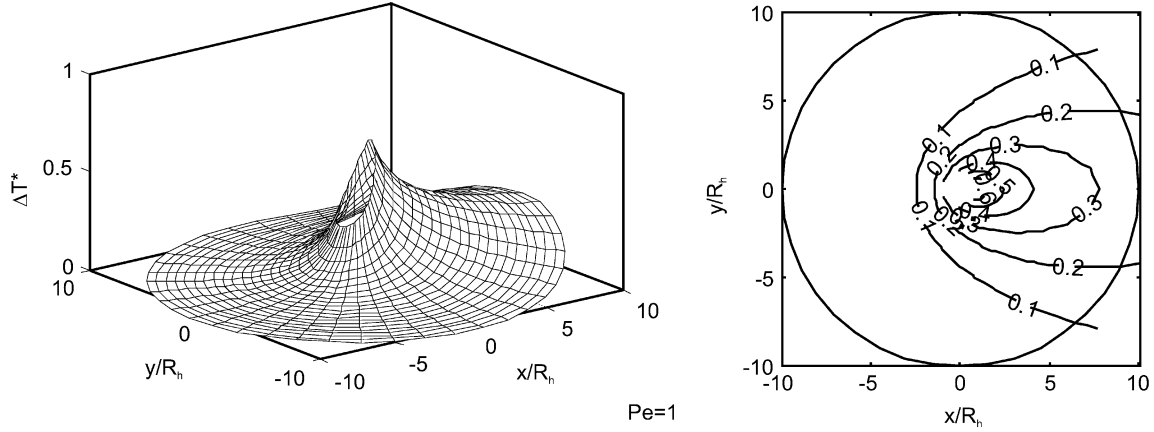


Fig. 2. Dimensionless temperature distribution at a constant linear heat rate and $Pe = 1$.

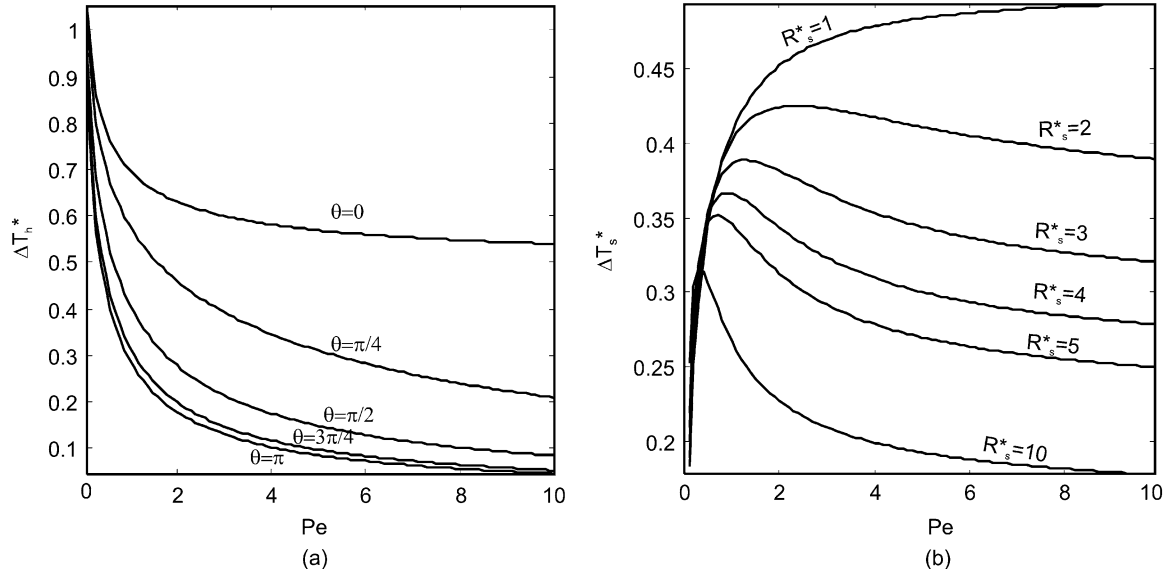


Fig. 3. Conventional thermal flow sensing methods at a constant heating power. (a) Hot-wire sensor—dimensionless heater temperature at different positions as a function of Peclet number. (b) Calorimetric sensor—dimensionless temperature difference between two positions upstream and downstream.

If Pe in (10) approaches 0, T_h^* approaches the asymptote $T_h^* = 1$. The temperature difference ΔT_s^* between the two positions 1 and 2 on the evaluation ring (Fig. 1) across the heater in flow direction is calculated as

$$\begin{aligned} \Delta T_s^* &= \Delta T_2^* - \Delta T_1^* \\ &= \Delta T^*(R_s^*, 0) - \Delta T^*(R_s^*, \pi) \\ &= \frac{K_0(Pe R_s^*/4)}{Pe} \left\{ \frac{\exp[Pe(R_s^* - 1)/4]}{K_1(Pe/4) - K_0(Pe/4)} \right. \\ &\quad \left. - \frac{\exp[-Pe(R_s^* - 1)/4]}{K_1(Pe/4) + K_0(Pe/4)} \right\} \end{aligned} \quad (11)$$

where $R_s^* = R_s/R_h$ is the dimensionless position of the temperature sensors. Since ΔT_h^* and ΔT_s^* are functions of Peclet numbers or the velocities of a given fluid, they can be used for measuring the 1-D flow. The corresponding methods are called the hot-wire anemometry and calorimetric anemometry, respectively [6]. The typical characteristics of the two methods are shown in Fig. 3

B. Temperature Field With a Constant Heater Temperature

Considering the constant temperature boundary condition, the solution for the temperature field is

$$\Delta T(r, \theta) = \Delta T_h \frac{K_0[vr/(2\alpha)]}{K_0[vR_h/(2\alpha)]} \frac{\exp[vr \cos \theta/(2\alpha)]}{\exp[vR_h \cos \theta/(2\alpha)]}. \quad (12)$$

By introducing the dimensionless temperature difference

$$\Delta T^* = \Delta T/\Delta T_h$$

the dimensionless temperature field at a constant heater temperature has the form

$$\Delta T^*(r^*, \theta) = \frac{K_0(Per^*/4)}{K_0(Pe/4)} \{ \exp[Pe(r^* - 1)/4] \}^{\cos \theta}. \quad (13)$$

Fig. 4 illustrates this result for different Peclet numbers. For the case of the flow sensor presented in this paper, the heat rate can be represented by the dimensionless Nusselt number. Assuming

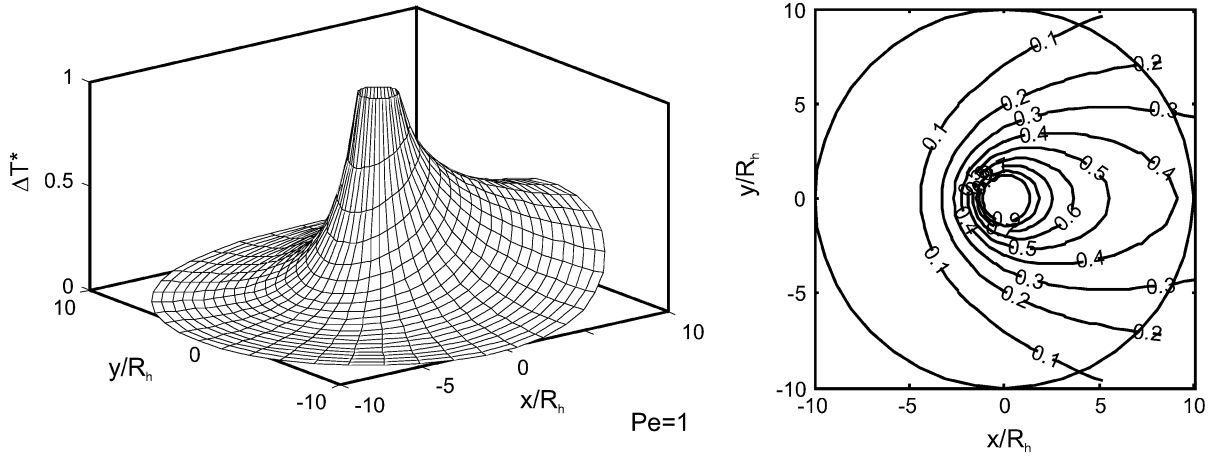
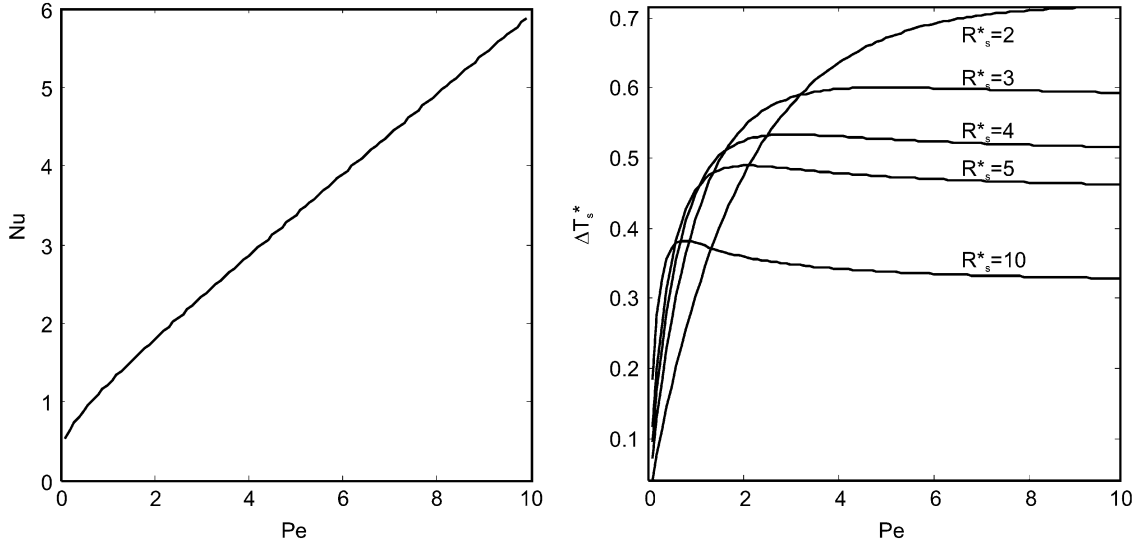

 Fig. 4. Dimensionless temperature distribution at a constant heater temperature and $Pe=1$.


Fig. 5. Conventional thermal flow sensing methods at a constant heater temperature. (a) Hot-wire sensor—Nusselt number as a function of Peclet number. (b) Calorimetric sensor—dimensionless temperature difference between two positions upstream and down stream.

a linear heat source q' and a characteristic length of $2R_h$, the Nusselt number Nu can be defined as

$$Nu = q' / (\pi k \Delta T_h). \quad (14)$$

Using the condition at the heater circumference

$$\frac{q'(\theta)}{2\pi R_h k} = - \left. \frac{dT(r, \theta)}{dr} \right|_{r=R_h} \quad (15)$$

the heat rate at the heater circumference is

$$q'(\theta) = \frac{\pi k \Delta T_h}{2} \left[\cos \theta - \frac{K_1(Pe/4)}{K_0(Pe/4)} \right]. \quad (16)$$

From (14), the average Nusselt number of the heater is

$$Nu = \frac{1}{\pi k \Delta T_h} \frac{1}{2\pi} \int_{-\pi}^{\pi} q'(\theta) d\theta = \frac{1}{2} Pe \frac{K_1(Pe/4)}{K_0(Pe/4)}. \quad (17)$$

Fig. 5 shows the relation between Nusselt numbers and Peclet numbers graphically.

The temperature difference between two positions upstream and down stream at a constant heater temperature is

$$\Delta T_s^* = \frac{K_0(Pe R_s^*/4)}{K_0(Pe/4)} \{ \exp[Pe(R_s^* - 1)/4] - \exp[-Pe(R_s^* - 1)/4] \}. \quad (18)$$

Both (17) and (18) are used in conventional hot-wire sensors and calorimetric sensors to determine the flow velocity, which is represented by the Peclet number (Fig. 5).

III. SENSING CONCEPTS AND EVALUATION ALGORITHMS

A. Evaluation of Direction

The new sensing concept presented in this paper is based on the temperature profile $\Delta T^*(R_s, \theta)$ along the circular path defined by R_s (Fig. 1). Using the dimensionless radius $R_s^* = R_s/R_h$ of the sensing path and considering an arbitrary flow direction θ_{flow} , the measured temperature profile along the circular path can be derived from (9) and (13).

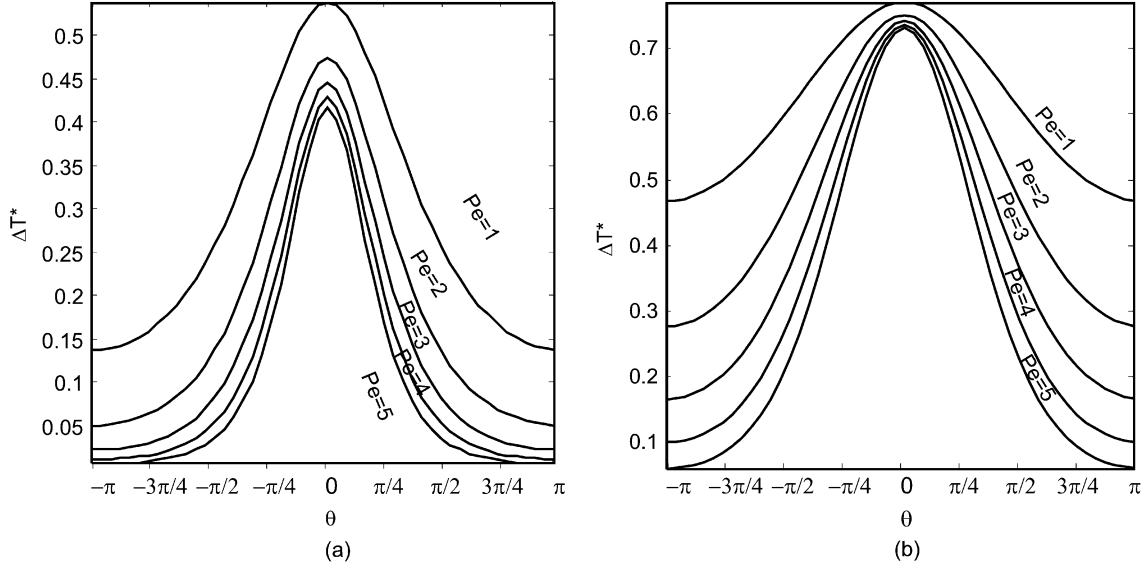


Fig. 6. Temperature profile on the circular sensing path at different Peclet numbers ($R_s^* = 2, \theta = 0$). (a) Constant heating power. (b) Constant heater temperature.

For a constant heating power, the temperature profile is

$$\Delta T^*(R_s^*, \theta) = \frac{A}{B - C \cos(\theta - \theta_{\text{flow}})} D^{\cos(\theta - \theta_{\text{flow}})}. \quad (19)$$

The temperature profile with a constant heater temperature has the form

$$\Delta T^*(R_s^*, \theta) = E \cdot D^{\cos(\theta - \theta_{\text{flow}})}. \quad (20)$$

The constants in (19) and (20) are defined as

$$A = K_0(\text{Pe} R_s^*/4)/\text{Pe}, \quad B = K_1(\text{Pe}/4), \quad C = K_0(\text{Pe}/4) \\ D = \exp[\text{Pe}(R_s^* - 1)/4], \quad E = K_0(\text{Pe} R_s^*/4)/K_0(\text{Pe}/4).$$

Fig. 6 shows the dimensionless temperature profiles along the circular evaluation path at different Peclet numbers. The temperature peak is sharper for the operation with a constant heating power or at higher Peclet numbers.

The measurement concept is based on the detection of three points on the temperature profile (19) and (20): $(\Delta T_1^*; \theta_1)$, $(\Delta T_2^*; \theta_2)$, and $(\Delta T_3^*; \theta_3)$. These three points can be detected by a temperature sensor array located on the sensing path, where the angular positions θ_n are fixed. The middle point $(\Delta T_2^*; \theta_2)$ has the maximum value, which can be detected by a maximum search function. The neighboring points $(\Delta T_1^*; \theta_1)$ and $(\Delta T_3^*; \theta_3)$ can be determined by the same search function. With these three data points, a system of three equations can be formulated and solved for the three unknown variables θ_{flow} , Pe , and R_s^* . However, only θ_{flow} can be solved explicitly,

and it is difficult to obtain an analytical formula for θ_{flow} from (19). The formula for θ_{flow} derived from (20) is (21), shown at the bottom of the page. The above formula can be used for determining the flow direction from the known positions of the temperature sensors $\theta_1, \theta_2, \theta_3$ and the measured values $\Delta T_1^*, \Delta T_2^*, \Delta T_3^*$.

B. Evaluation of Flow Velocity

As already mentioned, the three data points and the function of temperature profile $\Delta T^*(\theta)$ allow to establish a system of three equations for the three unknown variables θ_{flow} , Pe , and R_s^* . However, only θ_{flow} of the constant temperature mode can be solved analytically for a relatively simple explicit form. The flow velocity is represented by the Peclet number Pe , which is analytically difficult to solve for.

Conventional flow measurement methods utilize the characteristics shown in Figs. 3 and 5. These methods are basically categorized as the hot-wire method and the calorimetric method.

The hot-wire method measures the heater temperature at a constant heating power [Fig. 3(a)] or the heating power at a constant temperature [Fig. 5(a)]. This method allows measuring a wide range of flow velocities.

The calorimetric method measures the temperature difference between two symmetrical positions upstream and downstream of the heater. The advantage of this method is the high sensitivity at low Peclet numbers [7]. The drawback is that the method only works for a small flow range corresponding to the ascending part of its characteristics [Figs. 3(b) and 5(b)].

$$\theta_{\text{flow}} = \arctan \left[\frac{-\frac{\ln(\Delta T_1^*/\Delta T_2^*)}{\ln(\Delta T_2^*/\Delta T_3^*)}(\cos \theta_2 - \cos \theta_3) + \cos \theta_1 - \cos \theta_2}{\frac{\ln(\Delta T_1^*/\Delta T_2^*)}{\ln(\Delta T_2^*/\Delta T_3^*)}(\sin \theta_2 - \sin \theta_3) - \sin \theta_1 + \sin \theta_2} \right] \quad (21)$$

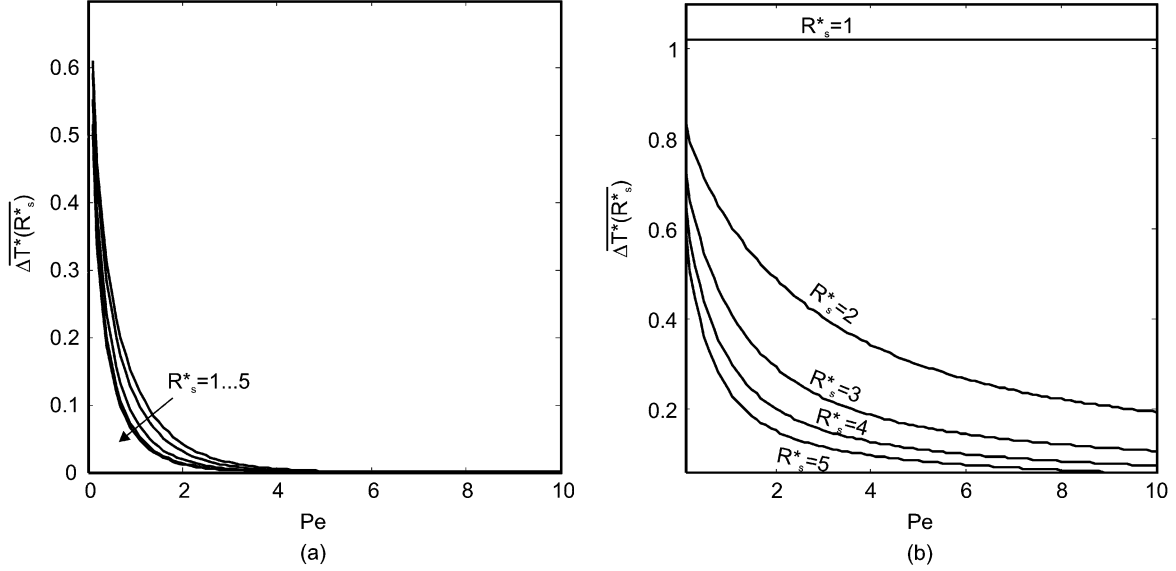


Fig. 7. Average temperature on the evaluation path with different dimensionless radii R_s^* . (a) Constant heating power. (b) Constant heater temperature.

With a measured temperature profile $\Delta T^*(R_s^*, \theta)$ on the circular path, the new sensor concept calibrates the flow velocity against the average temperature on sensing path

$$\overline{\Delta T^*}(R_s^*) = \frac{1}{2\pi} \int_{-\pi}^{\pi} \Delta T^*(R_s^*, \theta) d\theta. \quad (22)$$

The integration of (19) and (20) is analytically rigorous. Fig. 7 shows the results of the average temperature obtained numerically. The results show that the average temperature is well suited for determining the flow velocity.

IV. PARAMETRIC OPTIMIZATION

A. Optimization of Direction Measurement

The heater size R_h is an important parameter, which is already considered in the Peclet number. Thus, the three parameters for the optimization of the direction measurement are the Peclet number, the radial position R_s^* , and the angular position θ_n of the temperature sensors on the circular evaluation path.

Fig. 6 shows clearly that the direction measurement works better with a higher Peclet number. That means for a certain fluid, higher velocity results in a better direction measurement. Since the thermal diffusivity of gases is two order higher than those of liquids (e.g., at 300 K, the values for air and water are $\alpha_{\text{air}} = 2.21 \times 10^{-5} \text{ m}^2/\text{s}$, $\alpha_{\text{water}} = 1.43 \times 10^{-7} \text{ m}^2/\text{s}$); the direction measurement for liquids is better at the same velocity. Furthermore, based on its definition, a high Peclet number can also be achieved with a large heater radius.

The closer the radial position to the heater $R_s^* \rightarrow 1$, the higher the measured temperature. A high temperature compared to the ambient temperature will allow a higher signal-to-noise ratio (SNR). Thus, a closer position of the circular path is recommended.

For the evaluation concept discussed in Section III-A, at least three temperature sensors are needed for evaluating the direction. Theoretically, three temperature sensors on the evaluation path are able to detect the entire direction range from 0 to 2π .

However, the closer the three sensors, the higher the accuracy because of the higher signal-to-noise ratio.

B. Optimization of Velocity Measurement

As discussed in Section III-B, velocity measurement can be carried out in three ways: hot-wire method, calorimetric method, and the novel average-temperature method.

The characteristics of the hot-wire method are depicted in Figs. 3(a) and 5(a). The monotone characteristics shows that the higher temperature or heating power the better is the SNR. Since only the heater is involved in this method, no parametric optimization is necessary.

The characteristics of the calorimetric method depicted in Figs. 3(b) and 5(b) show highly nonlinear behaviors. The results show that this method is suitable for low Peclet numbers from 0 to 10. Equations (11) and (18) indicate that the two optimization parameters are the Peclet number Pe and the position R_s^* . Fig. 8 shows the dependence of the gradient $d(\Delta T_s^*)/dPe$ on the sensor position R_s^* at different Peclet numbers from 0.1 to 1. The results show clearly that the sensitivity of the calorimetric method, represented by the gradient $d(\Delta T_s^*)/dPe$ is higher for low Peclet number.

In the operation mode of constant heating power, the calorimetric characteristics is nonlinear over the entire range of sensor positions. For $Pe = 0.1$, there is a maximum of the gradient at $R_s^* \approx 5$. Thus, the optimal position for the temperature sensors is in the range $R_s^* \approx 1 \dots 5$.

In the operation mode of constant heater temperature, the calorimetric characteristics is almost linear for $R_s^* \rightarrow 1$. For the Peclet numbers depicted in Fig. 8(b), the optimal position of the temperature sensors is $R_s^* \approx 1.5 \dots 10$. However, if linearity is more important than sensitivity, the optimal position is $R_s^* \approx 1.5 \dots 2$.

The characteristics shown in Fig. 7(a) indicates that the method of average temperature $\overline{\Delta T^*}(R_s^*)$ at a constant heating power is suitable for the low range of Peclet numbers

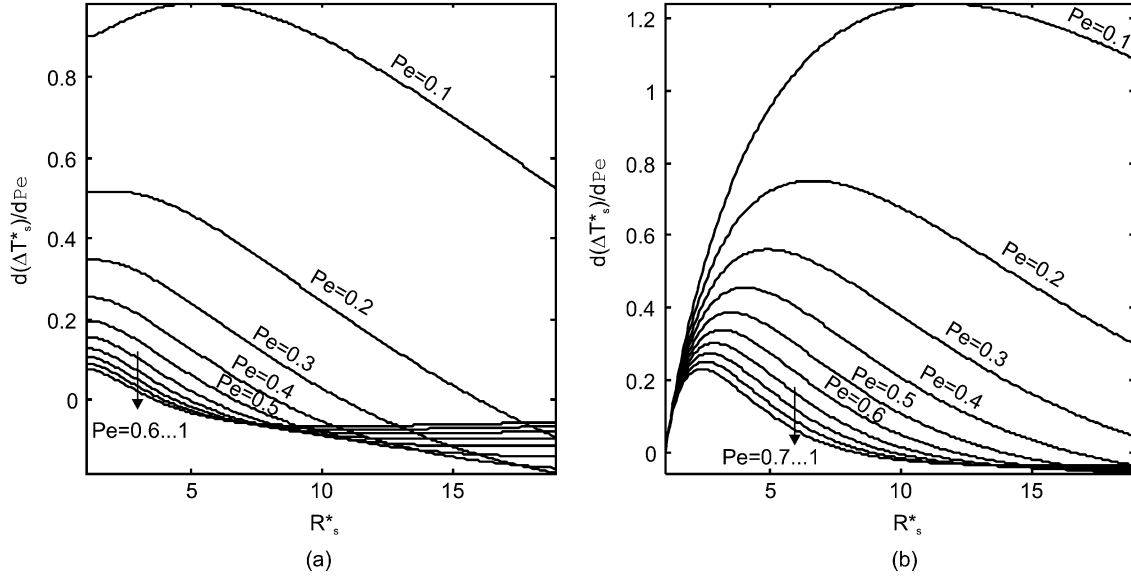


Fig. 8. Gradient of sensor characteristics of the calorimetric method at different Peclet numbers as a function of the dimensionless sensor position R_s^* . (a) Constant heating power. (b) Constant heater temperature.

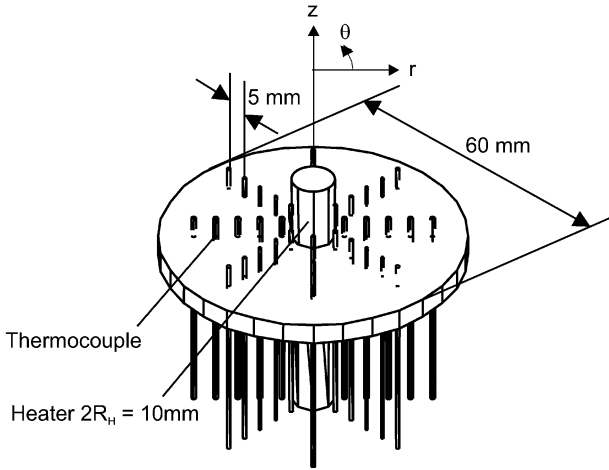


Fig. 9. Sensor prototype with a cylindrical heater and an array of temperature sensors.

($Pe = 0 \dots 1$). There is no significant difference in the characteristics with varying positions.

The characteristics of the average temperature $\overline{\Delta T^*}(R_s^*)$ at a constant heater temperature is suitable for a large range of Peclet numbers, Fig. 7(b). The sensitivity can be improved by placing the evaluation path further away from the heater.

V. SENSOR CONFIGURATION AND MEASUREMENT SET-UP

A. Sensor Configuration

The sensor prototype is designed as a disc. The heater and the array of temperature sensors are positioned on an aluminum disc. The disc measures 6 cm in diameter and has through holes for positioning the heater and temperature sensors. A cylindrical heat cartridge with a diameter of 1 cm is used as the heater. The heater contains a heating resistor and a K-type thermocouple, which allows feed-back control to keep the heater temperature constant. The heater is placed at the center of the disc with a thin

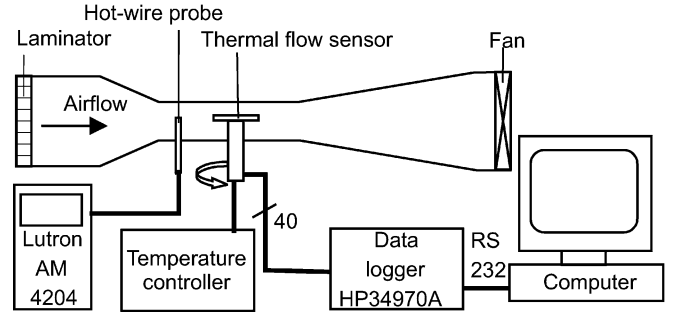


Fig. 10. Schematic concept of the measurement setup.

thermal insulator layer. K-type thermocouples are used as temperature sensors. In order to minimize the boundary layer effects and thermal coupling to the aluminum disc, the heater, and the temperature sensors stand 2 and 1 cm above the disc surface, respectively. The plastic wall around the thermocouple wires and the relatively long distance of 1 cm between the sensing point and the aluminum plate limit the thermal coupling effect of this plate. Fig. 9 shows the configuration of the prototype used for the experiments in this paper.

The sensing array consists of 40 temperature sensors located in a 5×8 array. There are five concentric evaluation paths with eight temperature sensors on each. The eight temperature sensors are positioned with an equal angular spacing of $\pi/4$. The innermost evaluation path has a diameter of $R_{s1} = 9.5\text{ mm}$. The other evaluation paths are placed radially 5 mm from each other. This configuration results to five different dimensionless sensor positions $R_s^* = R_s/R_h$ of 1.9, 2.9, 3.9, 4.9, and 5.9. The 40 thermocouples are connected to the multiplexer board of the data acquisition unit HP 34970A, which is in turn connected to a personal computer (PC) by the serial interface RS-232. The temperature profile above the disc is scanned and sent to the PC where the data is processed by programs written in MATLAB.

Before further evaluation, the measured temperatures are nondimensionalized against the heater temperature difference

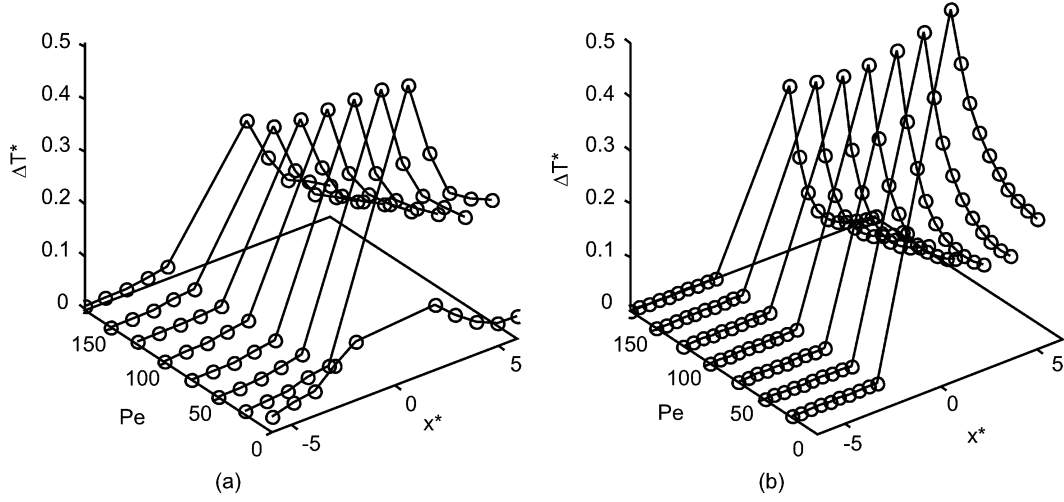


Fig. 11. Dimensionless temperature profile across the sensor in flow direction (experimental results versus analytical results $\Delta T = 100$ K). (a) Measurement. (b) Analytical model.

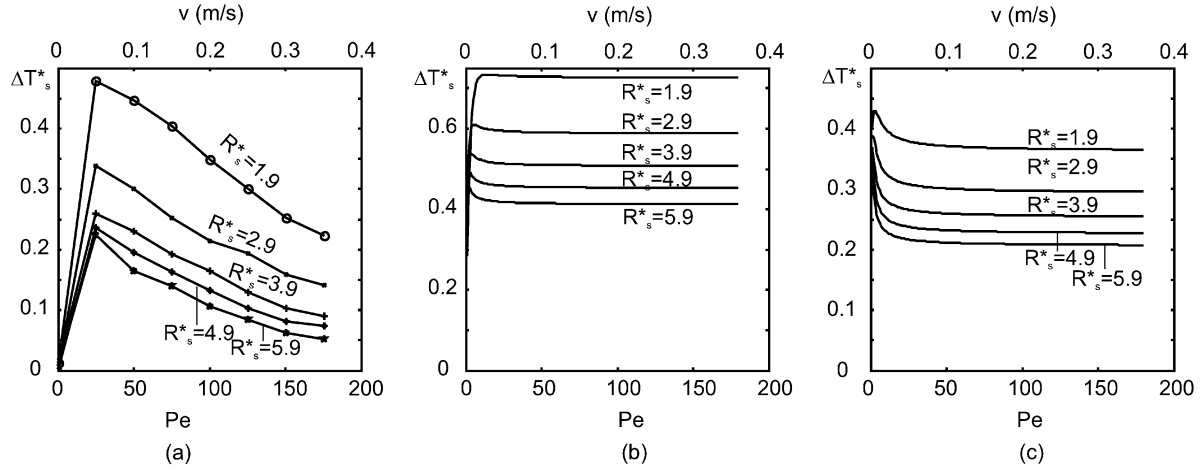


Fig. 12. Sensor characteristics in calorimetric mode (experimental results versus analytical results $\Delta T = 100$ K). (a) Measurement. (b) Analytical constant temperature. (c) Analytical constant heating power.

$\Delta T_h = T_h - T_0$, where T_h and T_0 are heater temperature and ambient temperature, respectively. The ambient temperature T_0 is calculated as the averaged value of all measured temperatures of the sensor array at nonheating condition

$$T_0 = 1/N \sum_{i=1}^5 \sum_{j=1}^8 T(i, j) \Big|_{\Delta T_h=0} \quad (23)$$

where $N = 40$ is the total number of temperature sensors and $T(i, j)$ is the temperature value of the element (i, j) in the array. The dimensionless temperature values can then be calculated as

$$\Delta T^*(i, j) = [T(i, j) - T_0] / [T_h - T_0]. \quad (24)$$

Results derived from $\Delta T^*(i, j)$ are used for detecting flow velocities and flow directions.

B. Measurement Setup

The measurement was carried out for air flow. Because of the relatively large size and the many wires connected to the flow sensor, the low-velocity measurement setup described in [7] could not be used. For the calibration of the flow velocity, a mini wind tunnel was used. The test section of the wind tunnel measures 10×20 cm. The flow velocity of the wind tunnel can be varied between 5 and 40 cm/s. The flow velocity was calibrated against a hot wire anemometer (Lutron AM-4204). Because of the heater size of $2R_h = 1$ cm, these relatively low air flow velocities lead to a range of Peclet numbers between 25 and 176. Thus, this experimental setup can not characterize the ascending part of the calorimetric characteristics [Figs. 3(b) and 5(b)].

The flow direction was emulated by rotating the flow sensor itself. A special attachment was designed to allow a positioning accuracy of about 1° or $\pi/180$. The measurements were carried out in an air-conditioned ambient, where the air temperature is kept constant at 23°C . The schematic and the actual experimental setup are shown in Fig. 10.

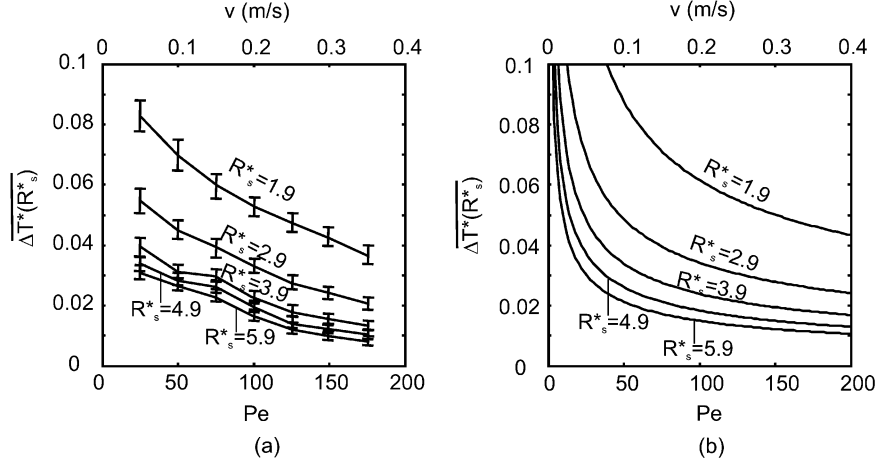


Fig. 13. Sensor characteristics of the average-temperature concept (experimental results versus analytical results $\Delta T = 100$ K). (a) Measurement. (b) Analytical constant heater temperature.

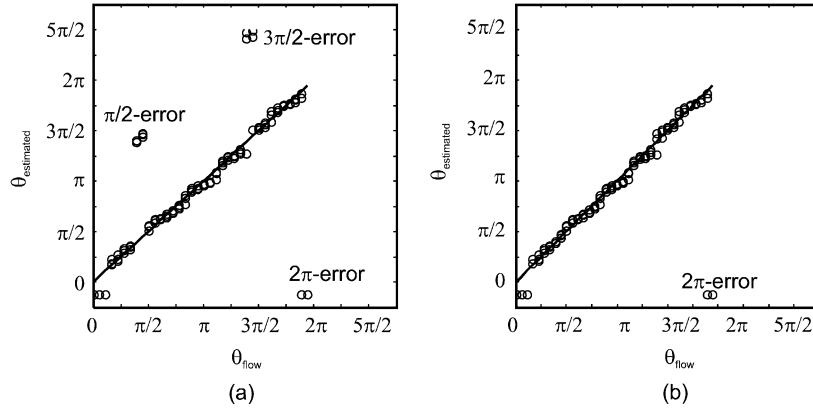


Fig. 14. Characteristic of direction measurement (experimental results, $\Delta T = 100$ K). (a) Using the analytical estimator. (b) Using the Gaussian estimator.

VI. EXPERIMENTAL RESULTS

A. Velocity Measurement

Since the heater temperature is kept constant at $\Delta T_h = 100$ K, there are two concepts for evaluating the flow velocity: the calorimetric concept for low velocity range and the time-average concept for the high velocity range.

With a heater diameter of 1 cm, the calorimetric concept is expected to work in the Peclet range less than 10 or for air velocities less than 1 cm/s. Because of the limitation of the experimental setup, which only allows the characterization of velocities more than 5 cm/s, only the descending part of the sensor characteristics can be evaluated.

Fig. 11 shows the temperature profile across the sensor in flow direction. Besides the slightly lower temperature as mentioned in the previous section, the measured results agree well with the analytical model. Fig. 12 shows the characteristics of the calorimetric concept with five different sensor pairs. As expected, only the descending part of the characteristics can be captured in the current experiments. The magnitude of the measured data is higher with a closer distance between the temperature sensors and the heater ($R_s^* \rightarrow 1$). This observation agrees with analytical results depicted in Fig. 12(b) and (c). However, the measurement shows a stronger cooling effect. Because of

the relatively low Reynolds number on the order of 100, the air flow remains laminar. The discrepancy can only be explained with the inhomogeneous heater temperature and the boundary layer effects which are neglected in the analytical model.

The average temperature on each of the five evaluation paths is calculated as

$$\overline{\Delta T^*(i)} = \frac{1}{8} \sum_{j=1}^8 T^*(i, j). \quad (25)$$

The characteristics of the average-temperature concept is shown in Fig. 13. The experimental results [Fig. 13(a)] show the expected characteristics of the analytical results [Fig. 13(b)]. Evaluation paths closer to the heater yield a higher magnitude, while the sensitivity of all paths remains in almost the same order.

B. Direction Measurement

In the direction measurement, the flow directions were emulated by rotating the sensor relatively to the mean flow of the wind channel. The direction angle θ_{flow} was increased from 0 to 2π in a $\pi/18$ -step. Because the innermost evaluation path ($R_s^* = 1.9$) always has the highest temperature, only their temperature sensors are chosen in this experiment for evaluation of the flow direction.

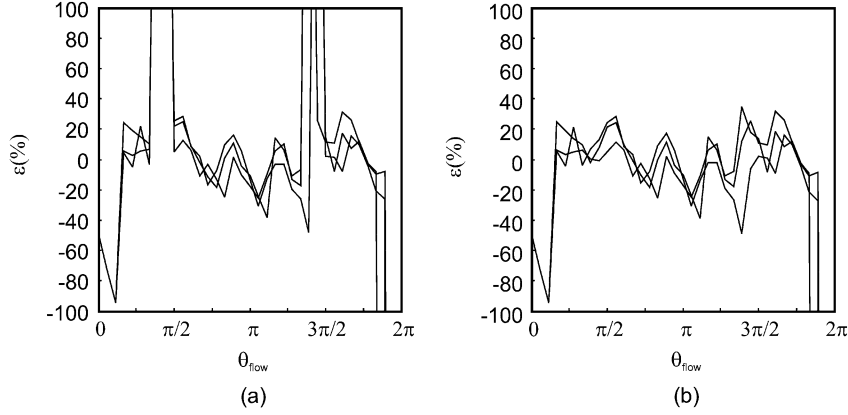


Fig. 15. Relative error of direction measurement (experimental results, $\Delta T = 100$ K). (a) Using the analytical estimator. (b) Using the Gaussian estimator.

The general evaluation algorithm starts with a search for the temperature peak of the eight measured values of the evaluation path. After determining the position of the temperature peak $(\theta_2, \Delta T_2^*)$ and its neighboring data points $(\theta_1, \Delta T_1^*)$ and $(\theta_3, \Delta T_3^*)$, the flow direction is determined by the estimator derived from the analytical model. The exact estimator (21) involves an arctan function which may have errors at $\theta_{\text{flow}} = \pi/2$ or $\theta_{\text{flow}} = 3\pi/2$, because, at these values, the tangent function of direction angle approaches infinity ($\tan(\theta_{\text{flow}}) \rightarrow \infty$).

Because of the above mentioned problems at $\theta_{\text{flow}} = \pi/2$ and $\theta_{\text{flow}} = 3\pi/2$, a simpler fitting function for the temperature peak can be used. With the direction angle θ , the fitting function $\Delta T^*(\theta)$ along the circular path can be described as a Gaussian distribution function

$$\Delta T^*(\theta) = \Delta T_{\text{max}}^* \exp \left[-\frac{(\theta - \theta_{\text{flow}})^2}{2\sigma^2} \right] \quad (26)$$

where ΔT_{max}^* , θ_{flow} and σ are the peak value, the corresponding direction angle at the peak, and the variance, respectively. With the three known measured points $(\theta_1, \Delta T_1^*)$, $(\theta_2, \Delta T_2^*)$ and $(\theta_3, \Delta T_3^*)$, the direction angle at the peak can be estimated as (27), shown at the bottom of the page. The variance σ and subsequently the maximum temperature difference ΔT_{max}^* can be estimated as

$$\sigma = \sqrt{\frac{(\theta_1 + \theta_2 - 2\theta_{\text{flow}})(\theta_2 - \theta_1)}{2 \ln(\Delta T_1^*/\Delta T_2^*)}} \quad (28)$$

$$\Delta T_{\text{max}}^* = \frac{\Delta T_1^*}{\exp \left[\frac{-(\theta_1 - \theta_{\text{flow}})^2}{2\sigma^2} \right]}. \quad (29)$$

Fig. 14 shows the measured direction angles with three set of data recorded at different flow velocities (5, 10, and 16.7 cm/s). The results show that the direction measurement is reproducible for different flow velocities. As expected, the results evaluated

with the analytical estimator show errors at $\theta_{\text{flow}} = \pi/2$ and $\theta_{\text{flow}} = 3\pi/2$, Fig. 14(a). However, these errors can be easily corrected by subtracting π from the evaluated angle. Since no trigonometric function is involved in the Gaussian estimator, the errors at $\theta_{\text{flow}} = \pi/2$ and $\theta_{\text{flow}} = 3\pi/2$ do not exist, Fig. 14(b). Both estimators show problems at $\theta_{\text{flow}} = 0$ and $\theta_{\text{flow}} = 2\pi$ because both angles represent the same flow direction. Fig. 15 compares the two estimators in terms of the relative errors of the direction measurements. The relative error (percentage) is defined as

$$\varepsilon = (\theta_{\text{flow},m} - \theta_{\text{flow},a})/(\pi/4) \times 100\% \quad (30)$$

where $\theta_{\text{flow},m}$ and $\theta_{\text{flow},a}$ are the measured direction angle and the actual direction angle respectively. The relative error represents the ratio between the measurement uncertainty and the geometrical resolution $\pi/4$. The actual direction angle has a relative error of 2.5% due to uncertainties of the rotation attachment. A relative error of about $\pm 20\%$ shows that the estimators improve the geometrical resolution by about five times. Compared to the absolute error of $\pm 2^\circ$ [8] and $\pm 5^\circ$ [9] of the micro-machined counterparts using two-sensor concepts, the absolute error of $\pm 9^\circ$ of the prototype is relative high. However, one should note that the absolute error can be further minimized by:

- using smaller geometrical resolution or more temperature sensor array;
- using micromachining which allows a more precise positioning of the temperature sensors as in the current prototype.

The similarity of the relative errors of the two estimators show that a Gaussian estimator is well suited for determining the flow direction. More temperature sensors on the evaluation path will improve the measurement resolution.

$$\theta_{\text{flow}} = \frac{(\theta_2^2 - \theta_1^2) \ln(\Delta T_2^*/\Delta T_3^*) - (\theta_3^2 - \theta_2^2) \ln(\Delta T_1^*/\Delta T_2^*)}{2[(\theta_2 - \theta_1) \ln(\Delta T_2^*/\Delta T_3^*) - (\theta_3 - \theta_2) \ln(\Delta T_1^*/\Delta T_2^*)]} \quad (27)$$

VII. CONCLUSION

An unified theory for different thermal flow sensor concepts such as the hot-wire method and the calorimetric method has been presented. Both operation modes with a constant heating power and with a constant heater temperature are considered in the analytical model. A new flow sensing concept has been derived from this theory. The concept allows measuring both flow direction and flow velocity. Based on the analytical model, the design of a novel thermal flow sensor was derived. The sensor consists of a cylindrical heater and an array of temperature sensors positioned on a circular evaluation path around the heater. The data taken from the temperature sensors allow the prediction of both flow direction and flow velocity. An algorithm was developed for estimating the direction from a set of three data points. In this way, a full direction range from 0 to 2π can be obtained. A sensor prototype was developed and characterized to verify the analytical model. The temperature profile around a circular heater was measured with a 5×8 array of temperature sensors. The measured temperature profiles at different flow velocities and different direction angles agree well with the analytical results. Different concepts for measuring the flow velocities were evaluated experimentally. Due to the limit of the current measurement setup, only the descending part of the calorimetric characteristics can be evaluated. Measurement results show a stronger cooling effect and a higher sensitivity as predicted with the analytical model. Experimental results of the novel time-average concept agree well with the theory. The signal magnitude is higher with an evaluation path closer to the heater. The sensitivity of this concept does not depend on the distance between the evaluation path and the heater. The novel direction measurement concept was presented with two algorithms: the analytical estimator and the Gaussian estimator. Although the analytical estimator is derived from the exact theoretical model, it contains trigonometric functions which may cause problems in the later implementation with a digital signal processor or with a microcontroller. The Gaussian estimator is an empirical algorithm but shows a comparable accuracy in a simple implementation.

REFERENCES

- [1] J. A. Kleppe, J. G. Olin, and R. K. Menon, "Point velocity measurement," in *Mechanical Variables Measurement- Solid, Fluid, and Thermal*, J. G. Webster, Ed. Boca Raton, FL: CRC, 2000.
- [2] B. W. van Oudheusden and J. H. Huijsing, "Integrated flow direction sensor," *Sens. Actuators A*, vol. 16, pp. 109–119, 1989.
- [3] —, "An electronic wind meter based on a silicon flow sensor," *Sens. Actuators A*, vol. 21–23, pp. 420–424, 1990.
- [4] B. W. van Oudheusden, "Silicon thermal flow sensor with a two-dimensional direction sensitivity," *Meas. Sci. Technol.*, vol. 1, pp. 565–575, 1990.
- [5] A. F. P. van Putten, M. J. A. M. van Putten, and M. H. P. M. van Putten, "Silicon thermal anemometry: Developments and applications," *Meas. Sci. Technol.*, vol. 7, pp. 1360–1377, 1996.
- [6] N. T. Nguyen, "Micromachined flow sensors: A review," *Flow Meas. Instrum.*, vol. 8, pp. 7–16, 1997.
- [7] N. T. Nguyen, X. Y. Huang, and K. C. Toh, "Thermal flow sensor for ultra-low velocities based on printed circuit board technology," *Meas. Sci. Technol.*, vol. 12, pp. 2131–2136, 2001.
- [8] K. A. A. Makinwa and J. H. Huijsing, "A smart wind sensor using thermal sigma delta modulation techniques," *Sens. Actuators A*, vol. 97–98, pp. 15–20, 2002.
- [9] S. Kim, S. Kim, Y. Kim, and S. Park, "A circular-type thermal flow direction sensor free from temperature compensation," *Sens. Actuators A*, vol. 108, pp. 64–68, 2003.
- [10] D. Rosenthal, "The theory of moving sources and its application to metal treatment," *Trans. ASME*, vol. 68, pp. 849–866, Nov. 1946.
- [11] G. Chryssolouris, *Laser Machining: Theory and Practice*. New York: Springer, 1993.
- [12] A. Abramowitz and I. Stegun, *Handbook of Mathematical Functions*. New York: Springer, 1970.



Nam-Trung Nguyen (M'01) was born in Hanoi, Vietnam, in 1970. He received the Dip.Eng., Dr.Eng., and Dr.Eng.-habil. degrees from the Chemnitz University of Technology, Germany, in 1993, 1997, and 2004, respectively.

In 1998, he was a Postdoctoral Research Engineer with the Berkeley Sensor and Actuator Center, University of California, Berkeley. Currently, he is an Assistant Professor with the School of Mechanical and Production Engineering, Nanyang Technological University, Singapore. His research is focused on microfluidics and instrumentation for biomedical applications. He has published a number of research papers on microfluidics. His recent book *Fundamentals and Applications of Microfluidics* (Norwood, MA: Artech House, 2002), coauthored with S. Wereley, was published in October 2002.